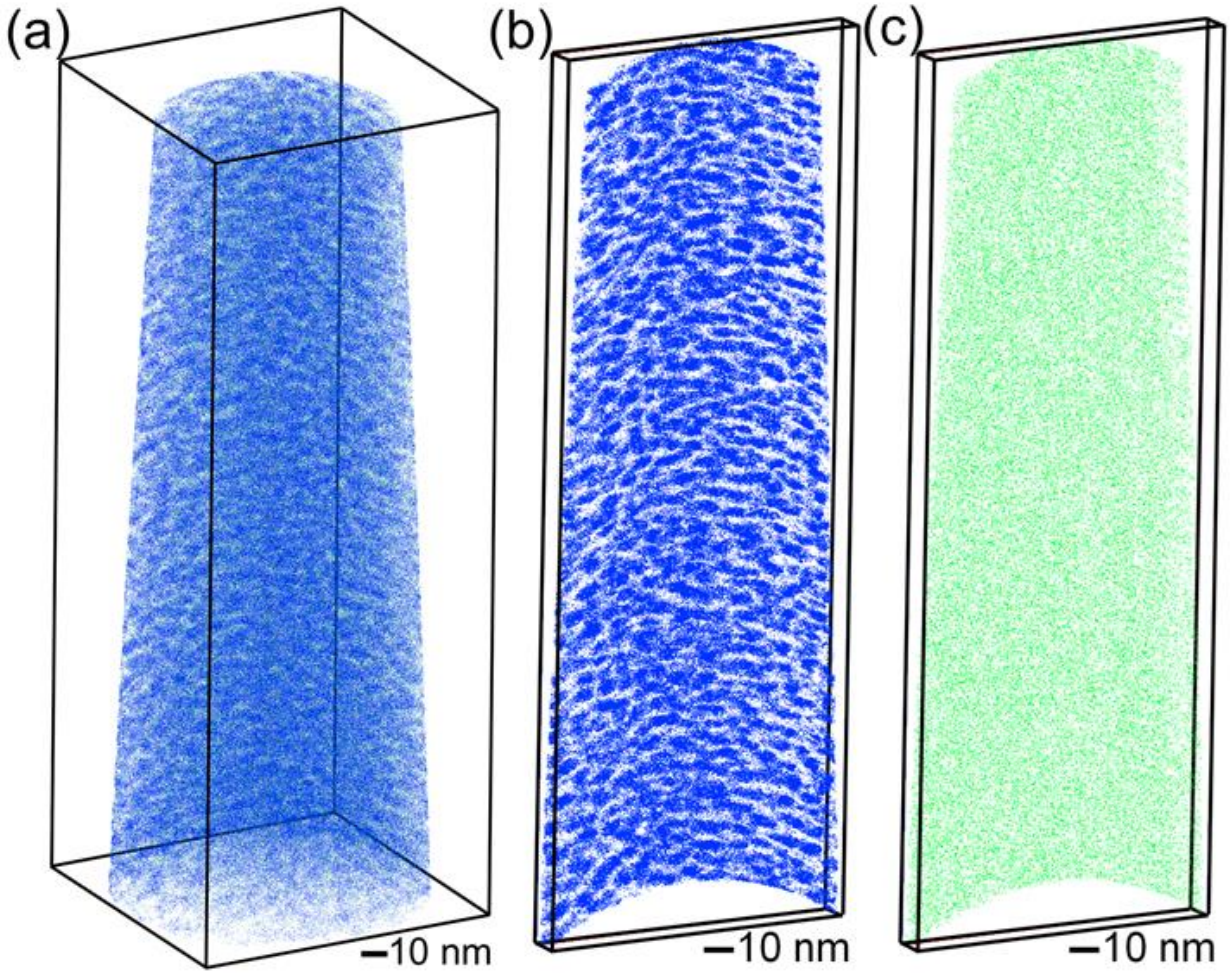

Supplementary Figure 1. Al-5.6Ag-0.84Cu (at. %) solution treated for 1 hour at 525ºC. (a) APT reconstruction containing $7.4x10^6$ atoms. Blue dots are Ag atoms, green dots are Cu atoms, Al atoms are not shown. (b) 10 nm slice of the reconstruction highlighting Ag distribution. (c) 10 nm slice of the reconstruction highlighting Cu distribution.

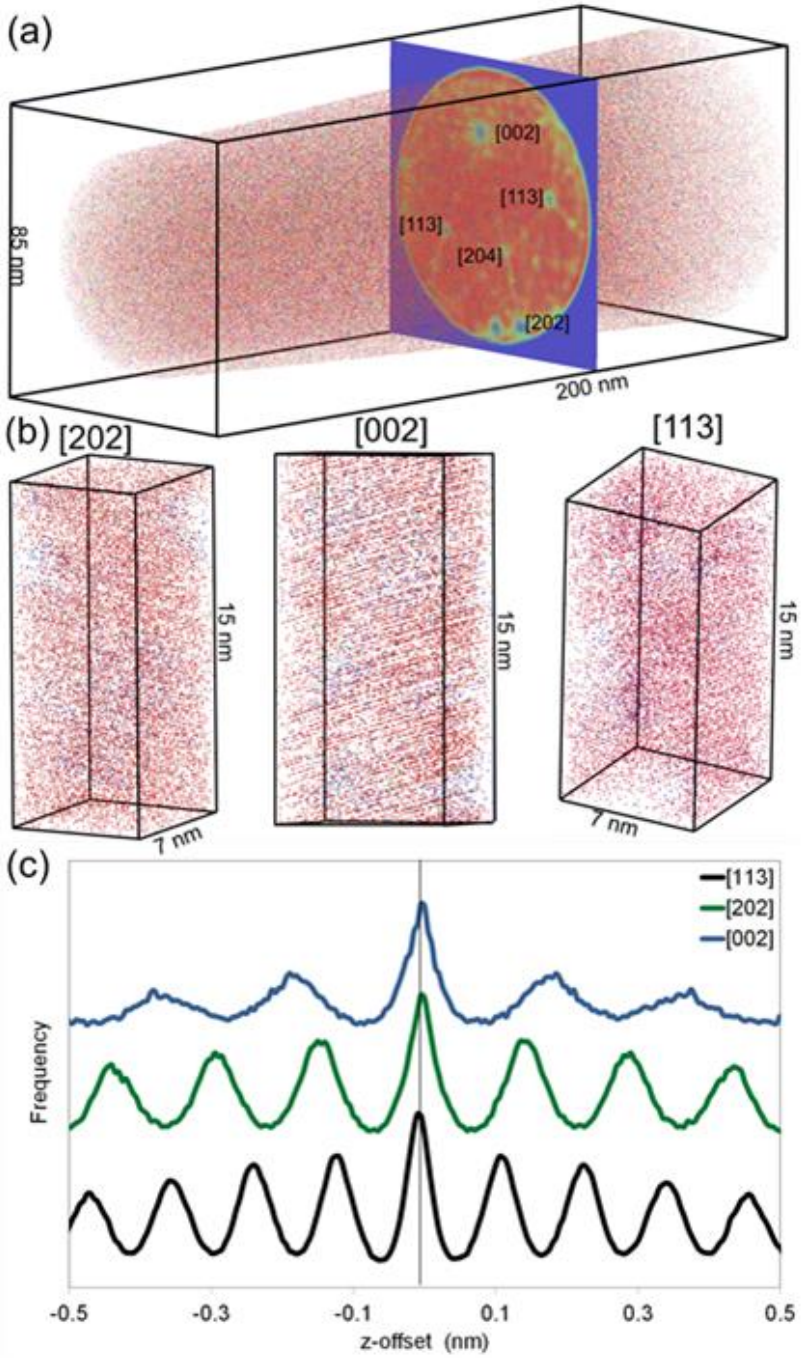

Supplementary Figure 2. Crystallographic information in APT reconstructions. (a) Al-Ag-Cu data from Supplementary Figure 1, Al atoms are now indicated as red dots. Superimposed is 2D map of density distributions in the x-y plane, highlighting a pattern of crystallographic poles. Poles have been indexed. (b) Small 7 x 7 x 15 nm regions of interest, taken from the vicinity of the [202], [002] and [113] poles respectively. Crystallographic planes are visible with appropriate tilting. (c) 1D distribution profiles in directions perpendicular to the direction of the planes in (b). Note that for clarity of comparison, distributions have been normalised and that the positions of the [202] and [113] distributions have been artificially raised above one another.

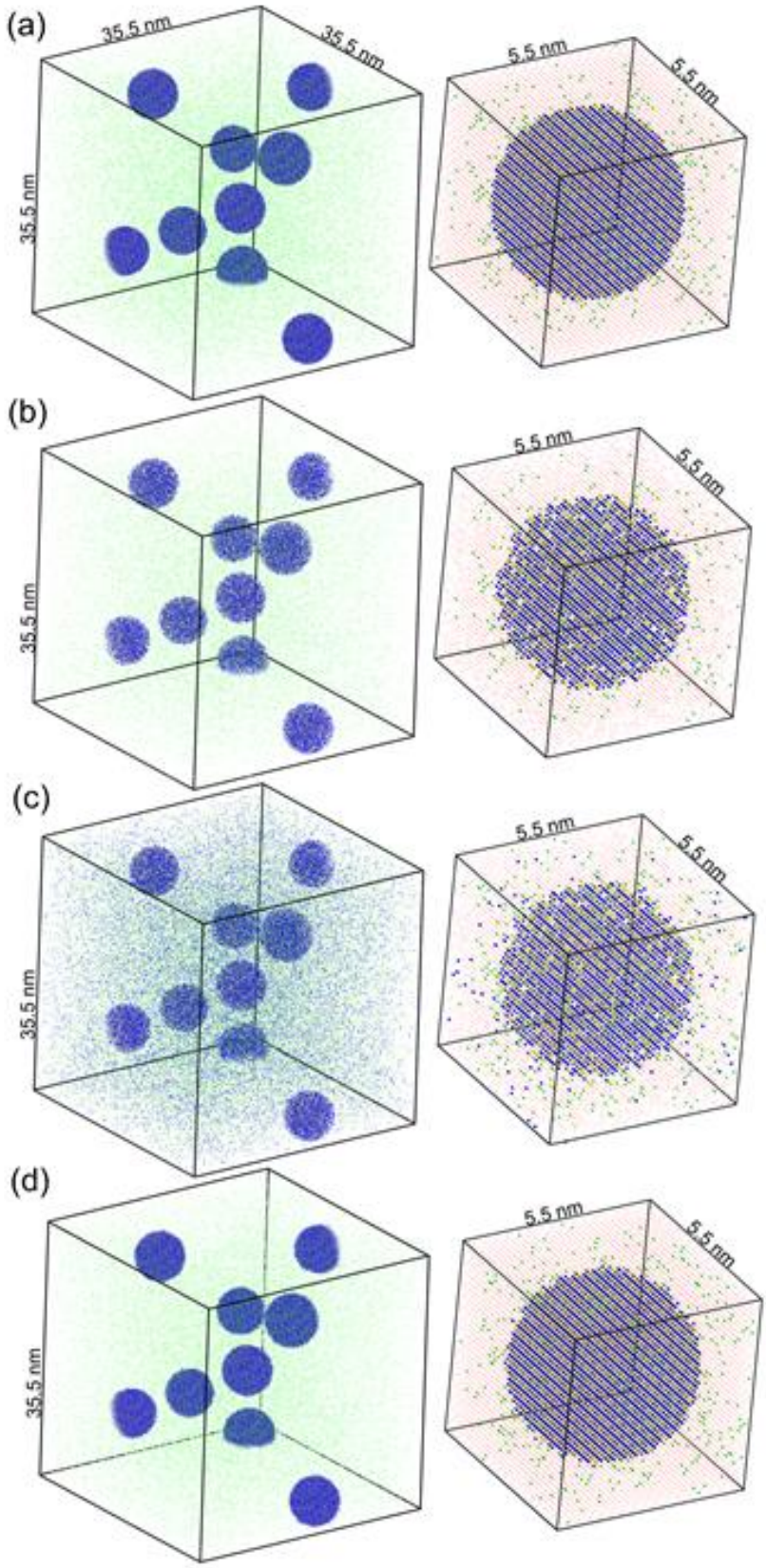
(a)
35.5 nm
35.5 nm
35.5 nm
5.5 nm
5.5 nm
(b)
35.5 nm
5.5 nm
5.5 nm
(c)
35.5 nm
5.5 nm
5.5 nm
(d)
35.5 nm
5.5 nm
5.5 nm

Supplementary Figure 3. Restoring the missing atoms to a simulated A-B-C-D quaternary system. (a) On left is original simulation (B-type atoms are green dots, C-type atoms are green, D-type atoms are yellow (matrix atoms (A) are not shown at this scale for sake of visual clarity) . On right is a close-up of a specific precipitate. Precipitates are comprised of C and D atoms and have a $L1_2$ structure. Matrix atoms are now shown and are now depicted by red dots. (b) Same simulation after 43% of atoms have been removed to model the effect of 57% detector efficiency. On right is corresponding close-up of same precipitate. (c) Atoms have been replaced at random into the vacant lattice sites. The overall composition of the system has been maintained. (d) The final system after distribution of the restored atoms is rearranged via MC simulation to return the original SRO. The structure of (a) has been maintained with an extremely high accuracy.

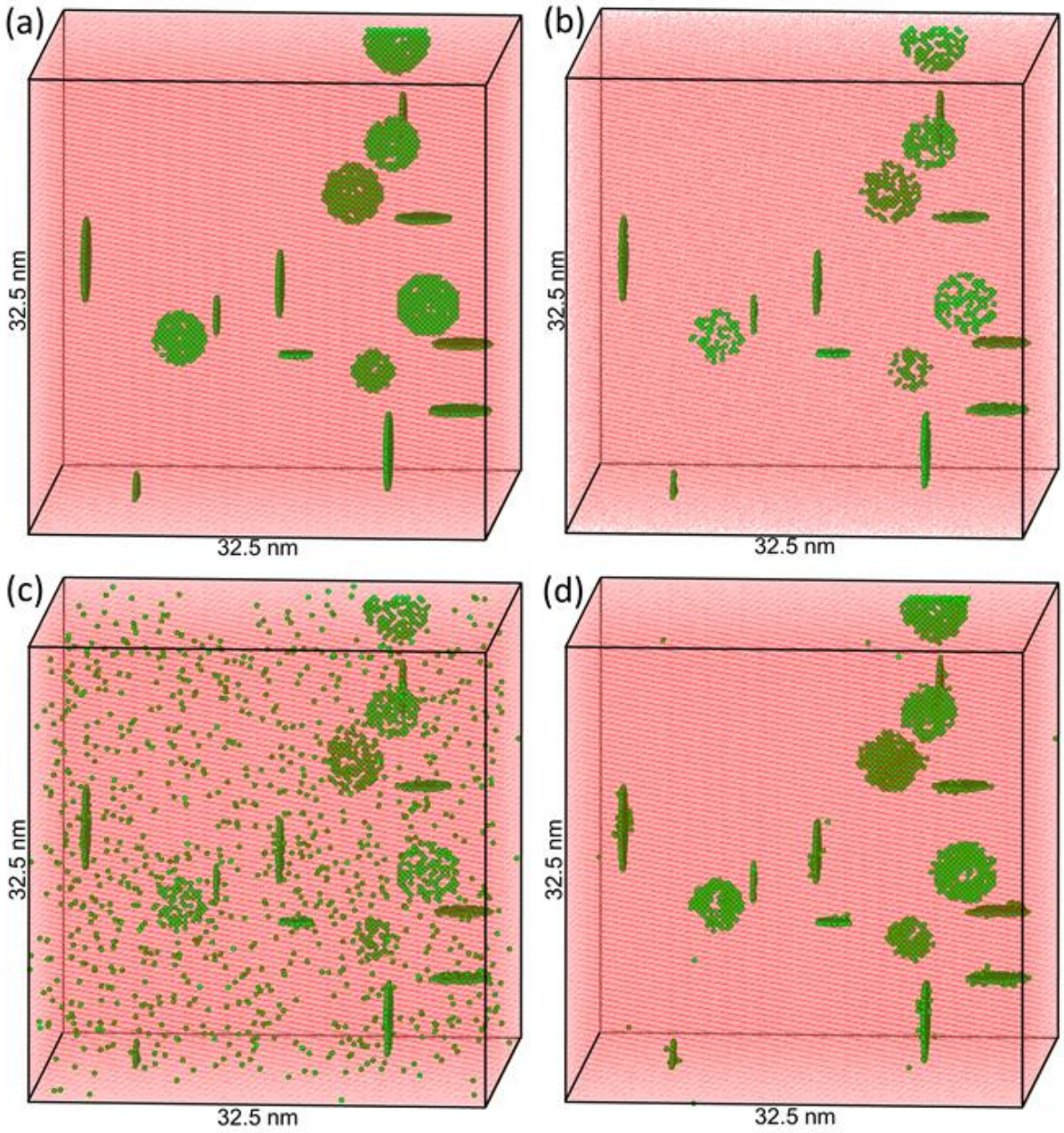

Supplementary Figure 4. Restoration of missing atoms to disc-shaped precipitates. (a) Simulated binary system, matrix atoms are represented by red dots and solute atoms by green spheres. All solute atoms are associated to single-layer disc shaped precipitates. (b) Same simulation after 43% of atoms have been removed to model the effect of 57% detector efficiency, as experienced in analysis via straight-ion-flight-path atom probe instruments. (c) Atoms have been replaced at random into the vacant lattice sites. The overall composition of the system has been maintained. (d) The final system after distribution of the restored atoms is rearranged via MC simulation to return the original SRO.

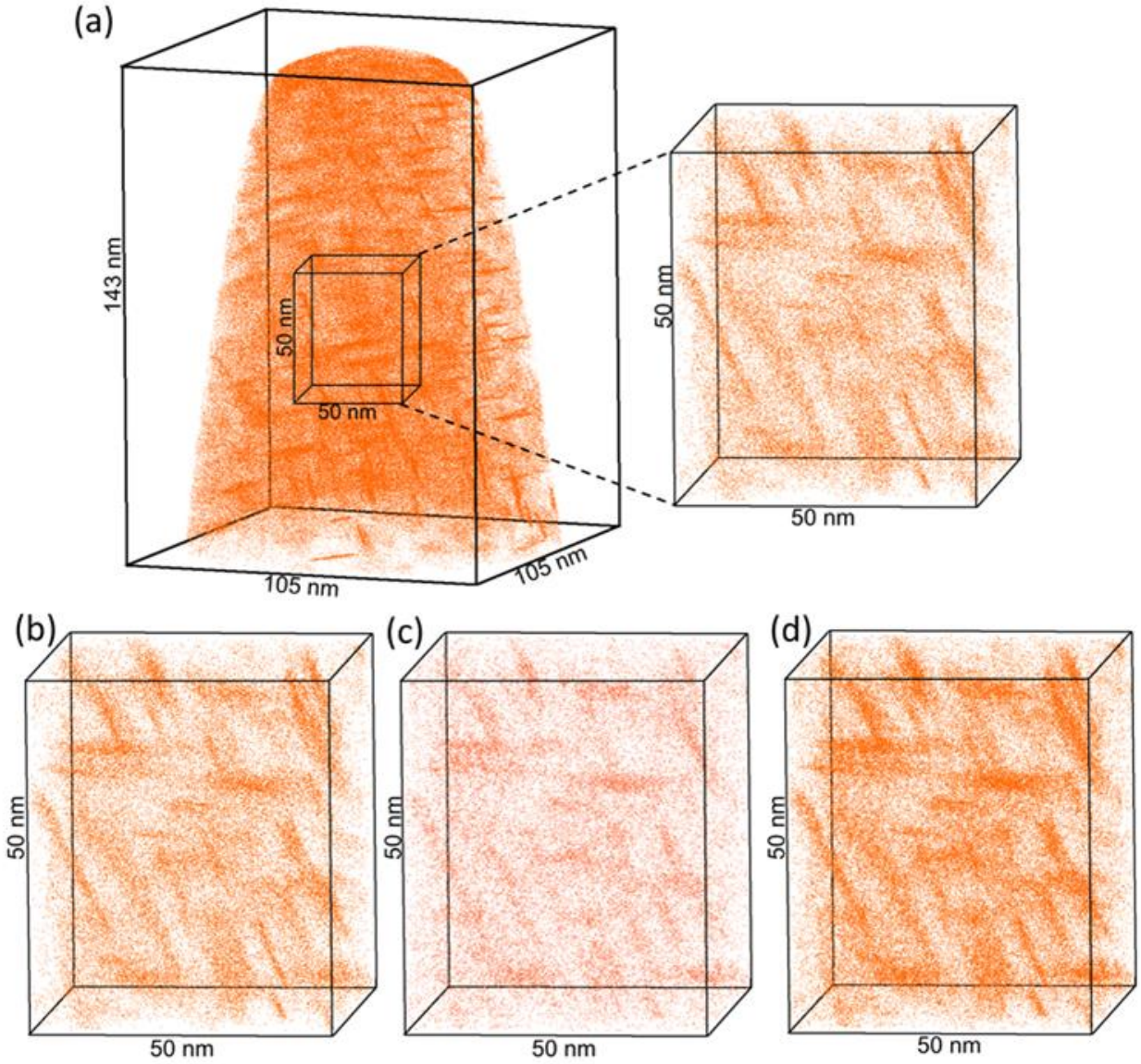

Supplementary Figure 5. Restoring atoms to plate-shaped precipitates. (a) Distribution of Cu atoms in Al-1.7Cu (at. %). Close-up of 50×50×40 nm region of interest containing ~ 3.5×10^6 atoms. (b) Lattice rectified region of interest from (a). (c) Distribution of missing atoms restored to the dataset. (d) Completed dataset combining original atoms from (b) and restored atoms from (c).

Supplementary Note 1: Crystallographic Information in Atom Probe Data

In atom probe tomography, atoms are individually removed from the surface of a very sharp needle-shaped specimen (with a radius at its apex of less than 50 nm) by the process of field evaporation [1]. To characterise ionic identity by time-of-flight mass spectrometry, an electric field is generated by the superimposition of a DC voltage and a high-voltage (HV) pulse or alternatively the HV pulse can be replaced with ultra-short laser pulses. The electric field at the apex of the specimen ionises the atoms and gives rise to a highly magnified projection of the ions onto a position-sensitive detector. Each hit on the detector can be directly related to the pulse responsible for the corresponding ionisation event, facilitating highly accurate time-of-flight measurements and mass resolutions. A reverse projection algorithm, combined with the sequence of evaporation and an assumed model for specimen shape enable a 3D atomistic reconstruction of the analysed volume[2].

Supplementary Figure 1 shows an atom probe reconstruction of an Al-5.6Ag-0.84Cu (at. %) alloy that has been solution treated for 1hour at 525ºC. The reconstruction incorporates 7.4 x 10^6 atoms, the 3D locations of which are represented by individual points in the reconstruction. The reconstructed data is electronic in nature, an ideal form for visualization and data-mining. In Supplementary Figure 1(a) the visualisation of Al atoms, the majority of the dataset, are simply not displayed, enhancing the visualisation of the distribution of the remaining solute atoms. In Supplementary Figures 1(b) and (c) the same virtual slice through the data has been highlighted showing the positions of the Ag and Cu atoms, respectively. The precipitation of the Ag atoms is in clear contrast to the apparently homogenous distribution of Cu atoms.

The spatial resolution of atom probe tomography is extremely high, estimated to be better than 0.06 nm in depth (*z*) and 0.20 nm laterally (*x and y*) [3-5]. However, the typical interatomic spacing is smaller than the lateral resolution, resulting in a significant loss of crystallographic information. Limited spatial resolution is due to a combination of trajectory aberrations in the flight path of the ions caused by local geometric and compositional variations on the surface of the specimen and the simplified model of the evaporation geometry in the 3D reconstruction.

Further, there is a random loss in detection efficiency due to limited open area of the microchannel plate (MCP) detectors, so that approximately 0.43 of the atoms evaporated from the specimen are randomly omitted from the final analysis. The fraction of atoms that strike the detector and are successfully detected is known as the detection efficiency, ε. For a flight straight path instrument $\varepsilon \approx 1-0.43 = 0.57$. However, the design of reflectron-fitted significantly reduces this value even further such that $\varepsilon \approx 0.37$[6].

Limited detection efficiency is a design limitation common to all commercial atom-probe detectors, with no existing practical instrumental solution. However, despite their exclusion from the data, the undetected atoms are taken into consideration in the creation of the tomographic reconstruction[2], meaning that high-precision inter-atomic distances between the detected atoms are still achieved. Moreover, the massive number of atoms accumulated in the experiment ($\sim 10^6 - 10^9$) allows for accurate composition statistics even at a very fine scale. Ultimately, the limited spatial resolution and detector efficiency prevent the direct analysis of crystallographic structure from current atom probe datasets.

Crystallographic information is not directly available within the APT reconstruction; however, it is not completely lost. Applied statistical techniques reveal that, collectively, atoms within the reconstruction can retain some crystalline structure of the original specimen, even though, individually, they are slightly scattered from their ideal lattice positions [7-10]. Supplementary Figure 2(a) shows the APT

dataset from Supplementary Figure 1. A region of interest has been highlighted and a 2D map highlighting the distribution of atomic densities within this region is shown. This map shows a pattern of small circular regions of low atomic density, corresponding to crystallographic poles, linked together by a series of 'zone lines', also of low atomic density. Each pole represents a set of major crystallographic planes, and hence crystallographic directions, in the face-centred cubic lattice of the analysed Al alloy, and the pattern in Supplementary Figure 2(a) can be appropriately indexed.

During the course of the experiment, the field evaporation in the vicinity of these poles takes place in a very controlled manner. After the experiment the reconstruction of the depth coordinates of individual atoms are assigned using an algorithm based upon the order in which they arrived at the detector. Controlled evaporation around the poles leads directly to the increase in resolution in the depth direction in the vicinity of the poles such to the extent that crystallographic planes can be observed [4]. In Supplementary Figure 2(b) small regions of interest around 3 respective crystallographic poles indicated in Supplementary Figure 2(a) are presented. With the appropriate tilt of the data the perspective can be optimized and crystallographic planes can be readily observed [11].

There are a number of ways for more rigorously identifying and characterising crystallographic planes present in 3D reconstructed APT data, such as Fourier Transformations [9], Hough Transformations[10] and spatial distribution maps (SDM) [7,8,12]. In this study we utilised SDM analyses. SDMs effectively split the 3D radial distribution into two components: a 1D distribution profile along a specific crystallographic direction and an associated 2D map of atomic distributions within a plane perpendicular to the 1D profile. As such the analysis builds a picture of average atomic neighbourhoods in the data set by directly examining inter-atomic offset vectors in the immediate vicinity of individual atoms.

For the purposes of this study only the information provided by the 1D profile component of the SDM analysis was necessary. Examples of SDM analyses corresponding to the respective sets of

crystallographic planes in Supplementary Figure 2(b) are presented in Supplementary Figure 2(c). In each graph the peak-to-peak distance represents the average plane spacing in that particular direction and the width of the peaks represents a measure of how accurately atoms are placed onto these planes. The plots are 1D distribution profiles, the vector defining these directions were obtained by systematically making a series of profiles in directions close to perpendicular to the observed atomic planes. The direction that produced a 1D distribution profile with the highest signal-to-noise ratio was deemed to be the most accurate measurement of the vector defining that crystallographic orientation. Vectors can be defined for each characterised crystallographic pole in the data and hence the angles between the reconstructed crystallographic directions can be measured with a high degree of accuracy.

In any given crystallographic direction characterised by the SDM analyses, atoms are not all distributed exactly on these crystallographic planes, resulting in the characteristic widths associated with the peaks in Supplementary Figure 2(c). However, we can apply a slight and very precise correction to their positions shifting each atom onto the closest lattice plane in a given crystallographic direction [13-16]. Critically, by re-mapping an atom simultaneously onto three independent sets of crystallographic planes identified in the data, its corrected position will be distinctly associated with the intersection of these planes, coinciding with a unique site on the perfect lattice. Using this approach, described in rigorous detail in reference [15] **,** it has been demonstrated that it is possible to restore the perfect face-centred cubic (FCC) or body-centred cubic (BCC) lattice of the original specimen to APT data. Due to the complex nature of the spatial resolution in APT data it can be difficult to quantify the accuracy of this procedure, however it was estimated that in a reasonable sized sub-volume of a pure Al reconstruction (containing more than 10^6 atoms) upwards of 85% of the rectified atoms were returned to the correct sites of the lattice.

Supplementary Note 2: Applications to more complex precipitates

A quaternary (*A*-*B*-*C*-*D*) system was simulated featuring precipitates exclusively containing *C*-type and *D*-type solute atoms arranged on a $L1_2$ structure (Supplementary Figure 3(a)). This configuration restricts the number of sites in the precipitate in which a *D*-type atom can be placed relative to the position of a *C*-type atom. The results show that based on an incomplete dataset, not only can atoms be accurately replaced back into a precipitate but the existing long-range order within these nanostructural features can be conserved.

This is not a trivial result. The SRO parameters are the only input informing the MC simulation. The results emphasize the fact that the probabilities of finding atoms in different crystallographic shells inherently contain information about the occupation of planes in different crystallographic orientations. It demonstrates what can be achieved by maximizing the amount of SRO information, particularly as a function of increasing crystallographic shell radius. In this case, characterization of the first five crystallographic shells was enough to conserve the $L1_2$ structure within the precipitates. This notion is further highlighted in the next example.

The capacity of this approach to reproduce the geometry of non-spherical nanostructural features was investigated. Based upon the well-known Guinier-Preston (GP) zones in thermally treated Al-Cu alloys, a simple simulated AB binary system was generated in which the solute atoms were distributed in the form of single-plane disc-shaped coherent precipitates on {002} habit planes of an FCC lattice. The results of randomly removing atoms from the system and then restoring the system utilising our SRO-based MC simulations are shown in Supplementary Figure 4 and are very encouraging. It can be seen that the majority of solute atoms are correctly restored to the plate-shaped precipitates. Some of the restored solutes are incorrectly replaced onto the surface of the precipitates, however, this number could be reduced with increased statistics and extending algorithm running times. This successful restoration of atoms to these non-spherical precipitates is another example in which complexity of

nanostructure is inherently contained in the SRO measurements. The solutes atoms have a preferred nearest neighbour distance within the {002} which is smaller than the distance to an adjacent plane. Hence when a solute atom is place on an adjacent plane, the distribution of neighbouring solutes is significantly different to the average distribution inherently contained in the SRO measurements.

This simulation results highlights three key strengths that underpin the approach

- Characterisation and application of SRO parameters for crystallographic shells of increasing radii
- Incorporation of not only solute-solute SRO parameters, but also solute-solvent and solvent-solvent distributions to drive the MC simulation
- Building upon the original incomplete data, rather than trying to recreate complex nanostructure by originally by simply seeding a completely random configuration of atoms into the MC simulation in the first step.

Supplementary Figure 5 is an APT reconstruction of a Al-1.7Cu (at.%) specimen which was solution treated then thermally aged for 4 hours at 100ºC. The formation of Cu GP zones in this system is very well documented and clearly apparent in Supplementary Figure 5(a) (Al atoms are not shown for visual clarity). A 50×50×40 nm ROI was isolated containing ~ 3.5×10^6 atoms (Supplementary Figure 5(b)) and the outlined steps for rectification of the lattice and restoration of the missing atoms (as described for the Al-Cu-Ag dataset) were applied. The distribution of the simulated restored Cu atoms generated by this is presented in Supplementary Figure 5(c) and the final corrected and completed hybrid dataset, containing both detected and simulated atoms, is given in Supplementary Figure 5(d). Again there is excellent agreement between the distribution of detected and simulated Cu atoms, as predicted by the simulations in Supplementary Figure 4.

Supplementary References

1 Kelly, T. F. & Larson, D. J. The second revolution in atom probe tomography. *MRS Bull.* **37**, 150-158 (2012).

2 Gault, B. *et al.* Advances in the reconstruction of atom probe tomography data. *Ultramicroscopy* **111**, 448-457 (2011).

3 Gault, B. *et al.* Spatial Resolution in Atom Probe Tomography. *Microscopy and Microanalysis* **16**, 99-110 (2010).

4 Gault, B. *et al.* Origin of the spatial resolution in atom probe microscopy. *Applied Physics Letters* **95**, 034103 (2009).

5 Cadel, E., Vurpillot, F., Larde, R., Duguay, S. & Deconihout, B. Depth resolution function of the laser assisted tomographic atom probe in the investigation of semiconductors. *Journal of Applied Physics* **106**, 044908 (2009).

6 Panayi, P. Great Britain Patent # GB2426120A. (2006).

7 Boll, T., Al-Kassab, T., Yuan, Y. & Liu, Z. G. Investigation of the site occupation of atoms in pure and doped TiAl/Ti3Al intermetallic. *Ultramicroscopy* **107**, 796-801 (2007).

8 Geiser, B. P., Kelly, T. F., Larson, D. J., Schneir, J. & Roberts, J. P. Spatial distribution maps for atom probe tomography. *Microscopy and Microanalysis* **13**, 437--447 (2007).

9 Vurpillot, F., De Geuser, F., Da Costa, G. & Blavette, D. Application of Fourier transform and autocorrelation to cluster identification in the three-dimensional atom probe. *Journal of Microscopy* **216**, 234-240 (2004).

10 Yao, L. *et al.* Crystallographic structural analysis in atom probe microscopy via 3D Hough transformation. *Ultramicroscopy* **111**, 458-463 (2011).

11 Warren, P. J., Cerezo, A. & Smith, G. D. W. Observation of atomic planes in 3DAP analysis. *Ultramicroscopy* **73**, 261-266 (1998).

12 Moody, M. P., Gault, B., Stephenson, L. T., Haley, D. & Ringer, S. P. Qualification of the tomographic reconstruction in atom probe by advanced spatial distribution map techniques. *Ultramicroscopy* **109**, 815-824 (2009).

13 Camus, P. P., Larson, D. J. & Kelly, T. F. A Method for reconstructing and locating atoms on the crystal lattice in 3-dimensional atom probe data. *Applied Surface Science* **87-8**, 305-310 (1995).

14 Vurpillot, F., Renaud, L. & Blavette, D. A new step towards the lattice reconstruction in 3DAP. *Ultramicroscopy* **95**, 223-230 (2003).

15 Moody, M. P. *et al.* Lattice Rectification in Atom Probe Tomography: Toward True Three-Dimensional Atomic Microscopy. *Microscopy and Microanalysis* **17**, 226-239 (2011).

16 Gault, B., Moody, M. P., Cairney, J. M. & Ringer, S. P. Atom probe crystallography. *Materials Today* **15**, 378-386 (2012).